HHS Public Access

Author manuscript

Anal Chem. Author manuscript; available in PMC 2023 June 29.

Published in final edited form as:

Anal Chem. 2023 May 23; 95(20): 8028–8035. doi:10.1021/acs.analchem.3c00919.

A General Method to Obtain Collision Cross Section Values in Multipass High-Resolution Cyclic Ion Mobility Separations

Sanaz C. Habibi,

Gabe Nagy

Department of Chemistry, University of Utah, 315 South 1400 East, Room 2020, Salt Lake City, Utah 84112, United States

Abstract

In recent years, ion mobility spectrometry-mass spectrometry (IMS-MS) has advanced the field of omics-based research, especially with the development of high-resolution platforms; however, these separations have generally been qualitative in nature. The rotationally-averaged ion neutral collision cross section (CCS) is one of the only quantitative metrics available for aiding in characterizing biomolecules in IMS-MS. However, determining the CCS of an ion for multipass IMS systems, such as in cyclic ion mobility-mass spectrometry (cIMS-MS) and structures for lossless ion manipulations (SLIM), has been challenging due to the lack of methods available for calculating CCS when more than a single pass is required for separation as well as the laborious nature of requiring calibrants and unknown compounds to be subjected to identical number of passes, which may not be possible in certain instances because of peak splitting, high levels of diffusion, etc. Herein, we present a general method that uses average ion velocities for calculating CCS values in cIMS-MS-based separations. Initially, we developed calibration curves using common CCS calibrants (i.e., TAAs, PolyAla, and HFAP) at different TW conditions and the calculated cIMS CCS values were within ~1% error or less compared to previously established DTIMS CCS measurements. Since it has been established that glycans can split into their α/β anomers, we utilized this method for two glycan species, 2α-mannobiose and melibiose. Both glycans were analyzed at the same TW conditions as the calibrants, and we observed anomer splitting at pathlengths of 20 m for 2α-mannobiose and 40 m for melibiose, and thus assigned two unique CCS values for each glycan, which is the first time this has ever been done. We have demonstrated that the use of average ion velocities is a robust approach for obtaining CCS values with good agreement to CCS measurements from previous literature and anticipate that this methodology can be applied to any IMS-MS platform that utilizes multipass separations. Our future work aims to incorporate this methodology for the development of a high-resolution CCS database to aid in the characterization of human milk oligosaccharides.

Graphical Abstract

Corresponding author: gabe.nagy@utah.edu.

Supporting Information

Average ion velocities, pathlengths used, example calculations, arrival time distributions of calibrants.

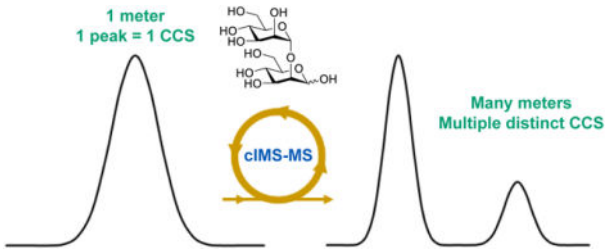

Introduction

Ion mobility spectrometry-mass spectrometry (IMS-MS) has emerged as a promising analytical technique for the analysis of many important biological molecules, especially in the omics (e.g., metabolomics, proteomics, glycomics, lipidomics, etc.).[1–4] In IMS-MS, ions are separated in the gas phase under the presence of an electric field based on their sizes, shapes, and charge (i.e., their ion mobilities).[1, 2, 5–7] Over the last decade, technological advancements have enabled higher resolution separations, such as in trapped IMS (TIMS), structures for lossless ion manipulations (SLIM), cyclic ion mobility spectrometry (cIMS), and field asymmetric ion mobility spectrometry (FAIMS), as compared to drift tube (DTIMS) measurements.[3, 8–34] We also note the use of cryogenic IR spectroscopy coupled to SLIM IMS-MS as a novel way to characterize various glycans.[35–41] Previous demonstrations using these high-resolution IMS-MS platforms have shown the ability to resolve many challenging molecular classes, with a specific emphasis on isomers.

While the ability to separate very structurally similar species with high-resolution IMS-MS, especially when it may not be possible via other analytical methods (e.g., liquid chromatography),[4, 32, 42] is of interest from an analytical perspective, a separation alone may not be enough to characterize an unknown molecule in a complex matrix. In DTIMS, a rotationally averaged ion-neutral collision cross section (CCS; Ω) can be directly calculated according to the Mason-Schamp relationship (Equation 1),[5, 6, 43] where μ is the reduced mass of the ion-neutral pair, k_b is Boltzmann's constant, ze is the ionic charge, N is the buffer gas number density, and K is the mobility of the ion. Unfortunately, due to the ~1-meter pathlength used in commercially-available DTIMS platforms, many isomers, or other structurally similar species, cannot be resolved and thus will have identical CCS values precluding identification of unknown compounds.[34, 44]

$$\Omega = \frac{3}{16}\sqrt{\frac{2\pi}{\mu k_b T}}\frac{ze}{NK} \quad (1)$$

In traveling wave-based (TWIMS) separations, CCS values cannot be directly calculated because of the non-linear relationship between arrival time and mobility.[45] Thus, to obtain CCS values in TWIMS calibrants, well-established CCS values from DTIMS measurements must be used. Traditionally, CCS values have been in good agreement between TWIMS and DTIMS demonstrating that the use of calibrant ions is a robust approach.[46, 47] However, TWIMS platforms that rely on increasing pathlength by cycling ions multiple passes around the device to improve resolution (e.g., SLIM IMS-MS and cIMS-MS) make it difficult

to calculate CCS values because of the wrap-around effect/ion lapping (i.e., where higher mobility faster species lap lower mobility slower ones). In SLIM IMS-MS, this is less of an issue since the commercially-available platform from MOBILion Systems is a single pass 13-meter pathlength,[44, 48] and thus no ion lapping can occur; it is important to mention that homebuilt SLIM IMS-MS platforms contain an ion switch that enables pathlengths of > 1 km.[23, 28, 49] In cIMS-MS, a single pass is 1-meter, where multiple passes generate the pathlengths (e.g., 10s of meters) required for the separation of challenging isomeric species.

Since prior to a given cIMS-MS separation it is unknown what pathlength is required to separate certain species, it is desirable to develop a pathlength independent methodology to enable CCS measurements. To the best of our knowledge, previous efforts on obtaining CCS values in cIMS-MS have exclusively focused on single pass, 1-meter, data.[15, 50, 51] But, it has clearly been demonstrated in previous literature that much longer pathlengths are required for the resolution of certain isomeric compounds thus 1-meter CCS data in cIMS-MS limits unknown identification.[9, 18, 29, 52–55] Since arrival time in cIMS-MS is pathlength dependent, the calibrant ions and ions of interest would each need to be subjected to the same number of passes, and a calibration curve would need to be constructed for each pass.[49] Additionally, this ignores the high probability, given the 1-meter peak capacity in cIMS-MS, that ions will lap one another, thus making arrival time meaningless. While slicing experiments can overcome ion lapping,[29, 53, 56] this has only been demonstrated on low complexity sample mixtures and thus new, general, methods are needed to address ion lapping in more complex matrices. Thus, our goal for this work was to present a general method to obtain pathlength independent CCS values without the previously mentioned laborious efforts required involving slicing experiments, generation of calibration curves for each pass, etc. Herein, we present the use of average ion velocities to establish a relationship to previously used CCS calibrant ions and thus enable CCS measurements in high-resolution, long pathlength/multipass, cIMS-MS separations. We envision that this approach is general in nature and can be readily adopted for any TWIMS-based platforms that require ion switching to increase pathlength and thus resolution. Our motivation for developing this method is to create a database of high-resolution cIMS-MS-based CCS values to increase confidence in the identification of human milk oligosaccharides (HMOs).

Materials and Methods

Reagents and Sample Preparation

Tetraalkylammonium salts (TAA3–8) were purchased from Santa Cruz Biotechnology (Dallas, Texas USA). Poly-DL-alanine (PolyAla) was purchased from Santa Cruz Biotechnology (Dallas, Texas USA) and an ESI low concentration tune mix containing hexakis(fluoroalkoxy)phosphazines (HFAP) was purchased from Agilent Technologies (Santa Clara, CA, USA). The disaccharides, 2α-mannobiose and melibiose, were purchased from Carbosynth (Berkshire, UK) and Sigma-Aldrich (Milwaukee, WI, USA), respectively. LC-MS grade solvents were obtained from Fisher Scientific (Pittsburgh, PA, USA). Stock solutions for all calibrant species and disaccharides were dissolved in 100% H_2O. Each TAA salt was prepared to 500 nM in a mixture in 49.75/49.75/0.5 (v/v) water/methanol/acetic acid. Poly-DL-alanine, 2α-mannobiose, and melibiose were prepared to 5 μM in

49.75/49.75/0.5 (v/v) water/methanol/acetic acid. The HFAP solution was diluted 10-fold in 95/5 (v/v) acetonitrile/water, with concentrations ranging from 50 to 100 nM.

Cyclic IMS-MS Conditions

The commercially-available cIMS-MS instrument by Waters Corporation (Wilmslow, UK) was utilized for all experiments.[53] All calibrants and glycan species were subjected to direct infusion electrospray ionization in positive-ion mode at a voltage of 2.5 kV with a flow rate of 2 μL/min for TAAs and PolyAla, and 5 μL/min for the HFAP mix, 2α-mannobiose, and melibiose. For all experiments, a quadrupole was used to *m/z* select ions of interest (i.e., each individual ion was selected from each calibrant mix to avoid unwanted ion lapping). Ions were then subjected to cIMS-MS separations in nitrogen buffer gas at 1.74 mbar and directed to the time-of-flight MS for detection in 'V' mode. Traveling wave (TW) conditions were optimized for each calibrant ion, and glycan species were analyzed at the same conditions as the calibrants. Please see figure and table captions for TW conditions used. It should be noted that maximum separation pathlengths for calibrants were determined by when the "wrap-around" effect was observed. Signal averaging for arrival time distributions was done for a minimum of 2 min for ions at shorter pathlengths, while ions at longer pathlengths, especially larger *m/z* ions, required averaging times of up to 10 min. No additional smoothing was performed. MassLynx and Quartz software were utilized for data acquisition and processing.

cIMS CCS Analysis

For all cIMS experiments, data acquisition was replicated over three days with a single data acquisition for the selected pathlengths each day. Arrival times were adjusted to account for only the time ions spend in the cyclic separation region (i.e., the dead time post cIMS-MS separation, or t_0, was subtracted out) as previously described.[57] Please see Table S1 and Equation 2 for a sample calculation, where $t_{corrected}$ is the corrected arrival time, n is the number of passes in meters, $t_{arrival}$ is the raw arrival time, and t_0 is the dead time post-cIMS-MS separation. Specifically, single and double pass (1 and 2 m) arrival time data was used to determine t_0, and as a result, the ion velocities at 1 and 2 m are identical. For specific pathlengths and individual ion velocities, please see Table S2 in the Supporting Information. Ion velocities were calculated using the apex of the peak from the corrected arrival times as well as pathlength in meters (i.e., the pathlength in meters was divided by the corrected arrival time to determine an ion's average velocity in meters per second). Reduced DTIMS CCS, Ω', values were calculated from previously reported ^{DT}CCS data[47, 58] using the relationship described in Equation 3,[49] where Ω is the reference ^{DT}CCS value from DTIMS under specific buffer gas, z is the charge of the ion, and μ is the reduced mass of the ion-neutral pair using nitrogen as the buffer gas. We note that the average ion velocities presented in Table 1 is representative of averaging the ion velocities over multiple pathlengths as well as the three interday trials (i.e., in total: 15 data points for each TAA, 12 data points for each PolyAla and HFAP). These averaged ion velocities and reduced DTIMS CCS values were then used to generate the calibration curves. Power regression models ($y = Ax^B$) have frequently been used for TWIM calibration curves, therefore, this trendline was applied for evaluating cIMS CCS in this work.[47, 49, 59, 60] Additionally, the power regression

model provided the best fit ($R^2 > 0.99$) for all calibrants compared to linear regression ($R^2 < 0.92$ for TAA / HFAP and < 0.98 for PolyAla).

$$t_{corrected} = nt_{arrival} - t_0 \quad (2)$$

$$\Omega' = \frac{\Omega}{z\sqrt{\frac{1}{\mu}}} \quad (3)$$

Results and Discussion

Use of Average Ion Velocities to Derive cIMS-Based CCS Values

CCS calibrants (Figure 1A), which included tetraalkylammonium salts (TAA), polyalanine (PolyAla), and hexakis(fluoroalkoxy)phosphazines (HFAP) were chosen due to their robustness, stability, ionization efficiency, ability to produce only a single IMS-MS peak, and use in previous literature.[47, 58, 59, 61, 62] Calibrant ranges for TAA (n = 3 – 8), PolyAla (n = 10 – 15), and HFAP (m/z 322 – 1822), where n represents alkyl chain length for the TAA and number of Ala in PolyAla, were selected to generate a wider m/z spread and allow for comparison between our derived cIMS-MS CCS values. As a first step, we subjected each set of calibrants to several meters of separation (Figures 1B and Figures S1–S3) to confirm that every ion generated only a single cIMS-MS peak. Since our overall motivation for developing a general method for calculating cIMS-based CCS values is to eventually develop a database for characterizing human milk oligosaccharides, each calibrant was only analyzed in positive mode as their common singly charged adducts (e.g., $[M + H]^+$ for the HFAP and PolyAla and [M+] for the TAA) because HMOs are predominantly detected as singly charged species in IMS-MS separations. Each calibrant set was analyzed at unique traveling wave conditions to ensure transmission of the entire m/z range as well as to ensure sufficient signal-to-noise across the various cIMS-MS pathlengths assessed. We were also interested in evaluating the effect of another traveling wave condition on our calculated CCS values and their respective errors. This is important because potential analytes of interest can have optimized traveling wave conditions other than those presented in this work, and thus necessitates our method to be robust across varying experimental conditions (i.e., reproducible CCS values and low errors regardless of traveling wave conditions).

Table 1 summarizes the traveling wave conditions used, m/z values, and calculated average ion velocities for each of the calibrants assessed. From Table 1, it can be observed that the percent relative standard deviation errors for average ion velocities were all on the order of < ~1% or less thus indicating that, as expected, average ion velocities at a given traveling wave condition is a pathlength independent metric. To calculate cIMS-based CCS values, we plotted reduced CCS values as determined from Equation 3 versus average ion velocities from Table 1 using power functions for each set of calibrants (Figure 2). In Figure 2, we observe R^2 values > 0.99 for each calibrant set under the traveling wave conditions assessed. Table 2 highlights our calculated cIMS-based CCS values for each set of calibrants as well as a comparison to previously published DTIMS CCS values (i.e., the same ones that

were used to determine our reduced CCS values).[47, 58] Our results not only demonstrate that the use of average ion velocities can be used to calculate CCS values on multipass high-resolution IMS-MS separations, but also that the two different traveling wave conditions used for the TAAs resulted in very similar calculated cIMS-based CCS values. Furthermore, we observe good agreement between our calculated cIMS-based CCS values and previously published DTIMS ones without any bias in one direction or the other (e.g., both positive and negative errors between cIMS and DTIMS CCS values were observed in Table 2). Overall, this demonstrates the utility of using ion velocities instead of absolute arrival times, which can become very convoluted because of ion lapping or peak splitting from multiple isomers/conformers being present, to derive CCS values on multipass IMS-MS separations.

Demonstration of High-Resolution cIMS-Based CCS Values for Glycan Analysis

As previously mentioned, our motivation for the development of a method to calculate CCS values in high-resolution cIMS-MS separations stems from the fact that many glycan isomers will be unresolved in a conventional 1-meter DTIMS experiment and thus have identical DTIMS-based CCS values. This precludes the ability to accurately characterize glycans in complex mixtures. As previously mentioned there have been many efforts related to separating glycan isomers in high-resolution IMS-MS, but these efforts have largely been qualitative in nature by only demonstrating that structurally similar species could be resolved rather than assigning any quantitative CCS value to them. Thus, the need for deriving CCS values in high-resolution multipass IMS-MS separations is at the forefront of the glycomics community. We envision that by being able to assign unique CCS values to each glycan isomer, or potentially multiple CCS values for an individual species based on their α/β anomers or other conformers, would better enable unknown identification.

Thus, to test our presented methodology for determining cIMS-based CCS values for glycans, we selected two species, 2α-mannobiose (α1,2 linkage between two mannose molecules) and melibiose (α1,6 linkage between galactose and glucose). Please see Figures 3 and 4 for their structures. Both of these glycans have previously been analyzed with other IMS-MS platforms (e.g., 1 m DTIMS and 25 cm TWIMS) and thus have published CCS values.[61–64] However, only one CCS value has been assigned for both 2α-mannobiose and melibiose even though it has been well established that glycans can split into their α/β anomers and/or open-ring conformations at higher IMS-MS resolutions. Thus, we were interested in assessing whether multiple peaks could be observed for these glycans when subjected to long pathlengths cIMS-MS separations as well as if we would be able to assign unique CCS values for each peak.

After a single pass, 1 m, cIMS-MS separation of the 2α-mannobiose (Figure 3A), only a single peak was observed. However, after 20 m of cIMS-MS separation, two peaks were observed which we attribute to be their α/β anomers based on previous literature.[9, 24, 32, 65, 66] For each of the traveling wave conditions sampled, we determined average ion velocities for both of the 2α-mannobiose peaks from triplicate trials performed on three independent days (see Table S3). From this, we calculated cIMS-based CCS values from our calibration curves in Figure 2. We would like to note that the unknowns (i.e., glycans in this work) must be analyzed at identical traveling wave conditions as the calibrant

species so that the relationship between ion velocity and reduced CCS, and thus CCS, would hold true. While this could potentially be laborious in certain instances because it would first require tuning the traveling wave conditions for the analytes/isomers of interest and then running the calibrants at the same traveling wave conditions, we reiterate that this is our approach to develop a CCS database in high-resolution multipass IMS-MS separations. Similarly, melibiose (Figures 4A and B) also exhibited a single IMS peak at 1 m and required a greater 40 m pathlength than 2α-mannobiose to resolve its α/β anomers. In Table 3, we display our calculated cIMS-based CCS values for each of the two peaks observed for both melibiose and 2α-mannobiose using the TAAs at varying traveling wave conditions and HFAP as calibrants. We did not use PolyAla as a calibrant for determining CCS values in these glycans for two reasons: 1) the *m/z* and reduced CCS range for the PolyAla calibrants we used would not bracket those for the glycans we analyzed and 2) the higher overall error observed for the PolyAla CCS values from Table 2 which we attribute to poorer signal-to-noise observed as indicated by slightly asymmetrical peak shapes (see Figure S2). When comparing our calculated cIMS-based CCS values for these glycans versus ones from previous literature, we observe error on the order of ~1–3% which has commonly been reported in comparing TWIMS versus DTIMS CCS values.[61–64] However, we reiterate that these previously reported CCS values were for a single peak owing to the lower resolution separations (i.e., shorter pathlengths), while our presented high-resolution cIMS-based ones clearly assign two distinct CCS values for both melibiose and 2α-mannobiose, presumably from their α/β anomers. We were also interested in comparing what the calculated, low-resolution, 1 m cIMS CCS value would be for each glycan versus those found for their anomers at higher resolution pathlengths. We found that the 1 m cIMS CCS values were 171.6 $Å^2$ and 174.9 $Å^2$ for 2α-mannobiose and melibiose, respectively, when using the TAAs as calibrants at traveling wave conditions of 450 m/s and 22 V. From this, it is observed that these 1 m cIMS CCS values fall are bracketed by the two cIMS CCS values calculated at longer pathlengths (i.e., 171.6 falls between 170.5 and 171.8 $Å^2$ for 2α-mannobiose and 174.9 falls between 174.3 and 175.0 $Å^2$; Table 3). Specifically, our CCS value for melibiose is in very good agreement with previously published TWIMS data using similar calibrants (Table 3).[62] While having multiple IMS peaks may seem like a negative outcome for glycan analyses, we view it as a positive one since it can increase confidence in characterization if an unknown glycan were to match up with two cIMS-based CCS values in a database. Lastly, we observed good agreement between our calculated cIMS CCS values regardless of what calibrant set was used, thus indicating robustness in our approach and enabling future adopters of this methodology to fine tune calibrants depending on their analyte needs.

It is important to discuss the scope and limitations of our presented method for calculating CCS values from average ion velocities in high-resolution cIMS-MS separations. Previous literature involving lipids has indicated that a systematic bias exists when comparing CCS values derived from DTIMS versus those from TWIMS in SLIM.[48] However, the key point was that CCS values must be first obtained from DTIMS allowing a comparison to TWIMS ones. This will not always be the case; for example, in the carbohydrate community there remains a lack of authentic analytical standards which would preclude obtaining DTIMS CCS values to correct for this bias in TWIMS. Nonetheless, CCS values have

been demonstrated to have high interlaboratory reproducibility with errors often < 1%. We envision our presented methodology being used in an internal database approach. By creating an internal database of cIMS-based CCS values, we envision developing improved methods for the characterization of human milk oligosaccharides. Additionally, we believe that the CCS values we derive in-house will have great lab-to-lab reproducibility amongst other cIMS-MS or SLIM IMS-MS users given both platforms utilize traveling wave-based separations, and could potentially be a subject for a community-wide led effort. Another potential drawback to our method is that it requires the CCS calibrants and analytes of interest to be subjected to identical TW conditions. Thus, we would recommend users optimize their separation first using the analytes of interest and then subjected the calibrants to those same experimental TW conditions. Lastly, we reiterate that an internal database approach will be the path moving forward with our presented CCS methodology and will require explicit description of calibrants and TW conditions used in order to disseminate this information to the IMS-MS community and enable more widespread adoption and interlaboratory reproducibility.

Conclusions

Herein we have presented a general method for calculating CCS values from high-resolution multipass IMS-MS separations by using average ion velocities rather than absolute arrival times. Our approach eliminates the laborious issue of creating calibration curves for each pathlength to determine absolute arrival times and furthermore overcomes the issue, and high likelihood, of ion lapping in the 1 m peak capacity of cIMS-MS separations. Our results demonstrate good agreement in our calculated cIMS-based CCS values with previously published DTIMS values for the various calibrant sets (e.g., HFAP, TAAs, and PolyAla) that we assessed. We expanded our methodology to analyze two glycans, 2α-mannobiose and melibiose, which both split into two peaks from their α/β anomers after 20 and 40 meters of cIMS-MS separation, respectively. This represents the first time that two distinct CCS values have been assigned for both of these glycans largely stemming from the fact that they have only been previously analyzed with lower resolution, and thus shorter pathlength, IMS-MS platforms which were unable to tease apart their anomers. We would like to note that the crucial aspect of our presented methodology is that in order to develop a database of cIMS-based CCS values, the analytes of interest and calibrant sets must be run at the same traveling wave conditions given that ion velocity is dependent on traveling wave amplitude and frequency. Since we analyzed our glycan species under multiple traveling wave conditions and with multiple CCS calibrants/CCS calibration curves, we believe that this demonstrates the robustness of our method given that our calculated CCS values were in good agreement regardless of calibrant and traveling wave conditions. We envision that our presented methodology is general enough in nature that it can readily be adopted by the IMS-MS community which rely on multipass separations for their analyses (e.g., SLIM or cIMS). Our overall goal moving forward is to develop a database of CCS values from our high-resolution cIMS-MS separations to better enable human milk oligosaccharide characterization. We also envision future potential collaborations with other cIMS or SLIM users to perform interlaboratory validation of our CCS values.

Supplementary Material

Refer to Web version on PubMed Central for supplementary material.

Funding Sources

The authors thank the University of Utah for startup funds and the National Institutes of Health (1R35GM146671–01).

References

(1). Burnum-Johnson KE; Zheng X; Dodds JN; Ash J; Fourches D; Nicora CD; Wendler JP; Metz TO; Waters KM; Jansson JK; et al. Ion mobility spectrometry and the omics: Distinguishing isomers, molecular classes and contaminant ions in complex samples. TrAC, Trends Anal. Chem 2019, 116 292–299.

(2). Paglia G; Smith AJ; Astarita G Ion mobility mass spectrometry in the omics era: Challenges and opportunities for metabolomics and lipidomics. Mass Spectrom. Rev 2022, 41 722–765. [PubMed: 33522625]

(3). Liu LC; Wang ZY; Zhang Q; Mei YQ; Li LN; Liu HW; Wang ZT; Yang L Ion Mobility Mass Spectrometry for the Separation and Characterization of Small Molecules. Anal. Chem 2023, 95 134–151. [PubMed: 36625109]

(4). Gaunitz S; Nagy G; Pohl NLB; Noyotny MV Recent Advances in the Analysis of Complex Glycoproteins. Anal. Chem 2017, 89 389–413. [PubMed: 28105826]

(5). Dodds JN; Baker ES Ion Mobility Spectrometry: Fundamental Concepts, Instrumentation, Applications, and the Road Ahead. J. Am. Soc. Mass Spectrom 2019, 30 2185–2195. [PubMed: 31493234]

(6). Gabelica V; Marklund E Fundamentals of ion mobility spectrometry. Curr. Opin. Chem. Biol 2018, 42 51–59. [PubMed: 29154177]

(7). Garimella SVB; Nagy G; Ibrahim YM; Smith RD Opening new paths for biological applications of ion mobility - Mass spectrometry using structures for lossless ion manipulations. TrAC, Trends Anal. Chem 2019, 116 300–307.

(8). Bowman AP; Abzalimov RR; Shvartsburg AA Broad Separation of Isomeric Lipids by High-Resolution Differential Ion Mobility Spectrometry with Tandem Mass Spectrometry. J. Am. Soc. Mass Spectrom 2017, 28 1552–1561. [PubMed: 28462493]

(9). Ujma J; Ropartz D; Giles K; Richardson K; Langridge D; Wildgoose J; Green M; Pringle S Cyclic Ion Mobility Mass Spectrometry Distinguishes Anomers and Open-Ring Forms of Pentasaccharides. J. Am. Soc. Mass Spectrom 2019, 30 1028–1037. [PubMed: 30977045]

(10). Huang YT; Dodds ED Discrimination of Isomeric Carbohydrates as the Electron Transfer Products of Group II Cation Adducts by Ion Mobility Spectrometry and Tandem Mass Spectrometry. Anal. Chem 2015, 87 5664–5668. [PubMed: 25955237]

(11). Nagy G; Chouinard CD; Attah IK; Webb IK; Garimella SVB; Ibrahim YM; Smith RD; Baker ES Distinguishing enantiomeric amino acids with chiral cyclodextrin adducts and structures for lossless ion manipulations. Electrophoresis 2018, 39 3148–3155. [PubMed: 30168603]

(12). Xie CY; Gu LC; Wu QD; Li L; Wang CL; Yu JC; Tang KQ Effective Chiral Discrimination of Amino Acids through Oligosaccharide Incorporation by Trapped Ion Mobility Spectrometry. Anal. Chem 2021, 93 859–867. [PubMed: 33226780]

(13). Fouque KJD; Ramirez CE; Lewis RL; Koelmel JP; Garrett TJ; Yost RA; Fernandez-Lima F Effective Liquid Chromatography-Trapped Ion Mobility Spectrometry-Mass Spectrometry Separation of Isomeric Lipid Species. Anal. Chem 2019, 91 5021–5027. [PubMed: 30896930]

(14). Fouque KJD; Garabedian A; Porter J; Baird M; Pang XQ; Williams TD; Li LJ; Shvartsburg A; Fernandez-Lima F Fast and Effective Ion Mobility-Mass Spectrometry Separation of D-Amino-Acid-Containing Peptides. Anal. Chem 2017, 89 11787–11794. [PubMed: 28982001]

(15). MacNeil A; Li XL; Amiri R; Muir DCG; Simpson A; Simpson MJ; Dorman FL; Jobst KJ Gas Chromatography-(Cyclic) Ion Mobility Mass Spectrometry: A Novel Platform for the Discovery of Unknown Per-/Polyfluoroalkyl Substances. Anal. Chem 2022.

(16). Hofmann J; Pagel K Glycan Analysis by Ion Mobility-Mass Spectrometry. Angew. Chem., Int. Ed 2017, 56 8342–8349.

(17). Chouinard CD; Nagy G; Webb IK; Shi TJ; Baker ES; Prost SA; Liu T; Ibrahim YM; Smith RD Improved Sensitivity and Separations for Phosphopeptides using Online Liquid Chromotography Coupled with Structures for Lossless Ion Manipulations Ion Mobility-Mass Spectrometry. Anal. Chem 2018, 90 10889–10896. [PubMed: 30118596]

(18). Williamson DL; Bergman AE; Nagy G Investigating the Structure of alpha/beta Carbohydrate Linkage Isomers as a Function of Group I Metal Adduction and Degree of Polymerization as Revealed by Cyclic Ion Mobility Separations. J. Am. Soc. Mass Spectrom 2021, 32 2573–2582. [PubMed: 34464117]

(19). Chouinard CD; Nagy G; Webb IK; Garimella SVB; Baker ES; Ibrahim YM; Smith RD Rapid Ion Mobility Separations of Bile Acid Isomers Using Cyclodextrin Adducts and Structures for Lossless Ion Manipulations. Anal. Chem 2018, 90 11086–11091. [PubMed: 30102518]

(20). Rathahao-Paris E; Delvaux A; Li MJ; Guillon B; Venot E; Fenaille F; Adel-Patient K; Alves S Rapid structural characterization of human milk oligosaccharides and distinction of their isomers using trapped ion mobility spectrometry time-of-flight mass spectrometry. J. Mass Spectrom 2022, 57.

(21). Nagy G; Kedia K; Attah IK; Garimella SVB; Ibrahim YM; Petyuk VA; Smith RD Separation of beta-Amyloid Tryptic Peptide Species with Isomerized and Racemized L-Aspartic Residues with Ion Mobility in Structures for Lossless Ion Manipulations. Anal. Chem 2019, 91 4374–4380. [PubMed: 30816701]

(22). Lane CS; McManus K; Widdowson P; Flowers SA; Powell G; Anderson I; Campbell JL Separation of Sialylated Glycan Isomers by Differential Mobility Spectrometry. Anal. Chem 2019, 91 9916–9924. [PubMed: 31283185]

(23). Deng LL; Webb IK; Garimella SVB; Hamid AM; Zheng XY; Norheim RV; Prost SA; Anderson GA; Sandoval JA; Baker ES; et al. Serpentine Ultralong Path with Extended Routing (SUPER) High Resolution Traveling Wave Ion Mobility-MS using Structures for Lossless Ion Manipulations. Anal. Chem 2017, 89 4628–4634. [PubMed: 28332832]

(24). Williamson DL; Bergman AE; Heider EC; Nagy G Experimental Measurements of Relative Mobility Shifts Resulting from Isotopic Substitutions with High-Resolution Cyclic Ion Mobility Separations. Anal. Chem 2022, 94 2988–2995. [PubMed: 35107996]

(25). Berthias F; Thurman HA; Wijegunawardena G; Wu HF; Shvartsburg AA; Jensen ON Top-Down Ion Mobility Separations of Isomeric Proteoforms. Anal. Chem 2022.

(26). Berthias F; Baird MA; Shvartsburg AA Differential Ion Mobility Separations of D/L Peptide Epimers. Anal. Chem 2021, 93 4015–4022. [PubMed: 33587599]

(27). Pathak P; Baird MA; Shvartsburg AA High-Resolution Ion Mobility Separations of Isomeric Glycoforms with Variations on the Peptide and Glycan Levels. J. Am. Soc. Mass Spectrom 2020, 31 1603–1609. [PubMed: 32501708]

(28). Wojcik R; Nagy G; Attah IK; Webb IK; Garimella SVB; Weitz KK; Hollerbach A; Monroe ME; Ligare MR; Nielson FF; et al. SLIM Ultrahigh Resolution Ion Mobility Spectrometry Separations of Isotopologues and Isotopomers Reveal Mobility Shifts due to Mass Distribution Changes. Anal. Chem 2019, 91 11952–11962. [PubMed: 31450886]

(29). Peterson TL; Nagy G Toward Sequencing the Human Milk Glycome: High-Resolution Cyclic Ion Mobility Separations of Core Human Milk Oligosaccharide Building Blocks. Anal. Chem 2021, 93 9397–9407. [PubMed: 34185494]

(30). Delvaux A; Rathahao-Paris E; Guillon B; Cholet S; Adel-Patient K; Fenaille F; Junot C; Alves S Trapped ion mobility spectrometry time-of-flight mass spectrometry for high throughput and high resolution characterization of human milk oligosaccharide isomers. Anal. Chim. Acta 2021, 1180.

(31). Miller SA; Fouque KJD; Ridgeway ME; Park MA; Fernandez-Lima F Trapped Ion Mobility Spectrometry, Ultraviolet Photodissociation, and Time-of-Flight Mass Spectrometry for Gas-Phase Peptide Isobars/Isomers/Conformers Discrimination. J. Am. Soc. Mass Spectrom 2022.

(32). Nagy G; Attah IK; Garimella SVB; Tang KQ; Ibrahim YM; Baker ES; Smith RD Unraveling the isomeric heterogeneity of glycans: ion mobility separations in structures for lossless ion manipulations. Chem. Commun 2018, 54 11701–11704.

(33). Pathak P; Baird MA; Shvartsburg AA Structurally Informative Isotopic Shifts in Ion Mobility Spectra for Heavier Species. J. Am. Soc. Mass Spectrom 2020, 31 137–145. [PubMed: 32881519]

(34). Deng LL; Ibrahim YM; Baker ES; Aly NA; Hamid AM; Zhang X; Zheng XY; Garimella SVB; Webb IK; Prost SA; et al. Ion Mobility Separations of Isomers based upon Long Path Length Structures for Lossless Ion Manipulations Combined with Mass Spectrometry. ChemistrySelect 2016, 1 2396–2399. [PubMed: 28936476]

(35). Ben Faleh A; Warnke S; Rizzo TR Combining Ultrahigh-Resolution Ion-Mobility Spectrometry with Cryogenic Infrared Spectroscopy for the Analysis of Glycan Mixtures. Anal. Chem 2019, 91 4876–4882. [PubMed: 30835102]

(36). Scutelnic V; Rizzo TR Cryogenic Ion Spectroscopy for Identification of Monosaccharide Anomers. J. Phys. Chem. A 2019, 123 2815–2819. [PubMed: 30829486]

(37). Khanal N; Masellis C; Kamrath MZ; Clemmer DE; Rizzo TR Cryogenic IR spectroscopy combined with ion mobility spectrometry for the analysis of human milk oligosaccharides. Analyst 2018, 143 1846–1852. [PubMed: 29541730]

(38). Ben Faleh A; Warnke S; Bansal P; Pellegrinelli RP; Dyukova I; Rizzo TR Identification of Mobility-Resolved N-Glycan Isomers. Anal. Chem 2022, 94 10101–10108. [PubMed: 35797429]

(39). Warnke S; Ben Faleh A; Scutelnic V; Rizzo TR Separation and Identification of Glycan Anomers Using Ultrahigh-Resolution Ion-Mobility Spectrometry and Cryogenic Ion Spectroscopy. J. Am. Soc. Mass Spectrom 2019, 30 2204–2211. [PubMed: 31520337]

(40). Pellegrinelli RP; Yue L; Carrascosa E; Ben Faleh A; Warnke S; Bansal P; Rizzo TR A New Strategy Coupling Ion-Mobility-Selective CID and Cryogenic IR Spectroscopy to Identify Glycan Anomers. J. Am. Soc. Mass Spectrom 2022, 33 859–864. [PubMed: 35437995]

(41). Bansal P; Yatsyna V; AbiKhodr AH; Warnke S; Ben Faleh A; Yalovenko N; Wysocki VH; Rizzo TR Using SLIM-Based IMS-IMS Together with Cryogenic Infrared Spectroscopy for Glycan Analysis. Anal. Chem 2020, 92 9079–9085. [PubMed: 32456419]

(42). Ruhaak LR; Lebrilla CB Advances in Analysis of Human Milk Oligosaccharides. Adv. Nutr 2012, 3 406s–414s. [PubMed: 22585919]

(43). Revercomb HE; Mason EA Theory of Plasma Chromatography Gaseous Electrophoresis - Review. Anal. Chem 1975, 47 970–983.

(44). May JC; Leaptrot KL; Rose BS; Moser KLW; Deng LL; Maxon L; DeBord D; McLean JA Resolving Power and Collision Cross Section Measurement Accuracy of a Prototype High-Resolution Ion Mobility Platform Incorporating Structures for Lossless Ion Manipulation. J. Am. Soc. Mass Spectrom 2021, 32 1126–1137. [PubMed: 33734709]

(45). Shvartsburg AA; Smith RD Fundamentals of Traveling Wave Ion Mobility Spectrometry. Anal. Chem 2008, 80 9689–9699. [PubMed: 18986171]

(46). Hinnenkamp V; Klein J; Meckelmann SW; Balsaa P; Schmidt TC; Schmitz OJ Comparison of CCS Values Determined by Traveling Wave Ion Mobility Mass Spectrometry and Drift Tube Ion Mobility Mass Spectrometry. Anal. Chem 2018, 90 12042–12050. [PubMed: 30215509]

(47). Hines KM; May JC; McLean JA; Xu LB Evaluation of Collision Cross Section Calibrants for Structural Analysis of Lipids by Traveling Wave Ion Mobility-Mass Spectrometry. Anal. Chem 2016, 88 7329–7336. [PubMed: 27321977]

(48). Rose BS; May JC; Reardon AR; McLean JA Collision Cross-Section Calibration Strategy for Lipid Measurements in SLIM-Based High-Resolution Ion Mobility. J. Am. Soc. Mass Spectrom 2022.

(49). Li AL; Conant CR; Zheng XY; Bloodsworth KJ; Orton DJ; Garimella SVB; Attah IK; Nagy G; Smith RD; Ibrahim YM Assessing Collision Cross Section Calibration Strategies for Traveling

Wave-Based Ion Mobility Separations in Structures for Lossless Ion Manipulations. Anal. Chem 2020, 92 14976–14982. [PubMed: 33136380]

(50). Higton D; Palmer ME; Vissers JPC; Mullin LG; Plumb RS; Wilson ID Use of Cyclic Ion Mobility Spectrometry (cIM)-Mass Spectrometry to Study the Intramolecular Transacylation of Diclofenac Acyl Glucuronide. Anal. Chem 2021, 93 7413–7421. [PubMed: 33984239]

(51). Richardson K; Langridge D; Dixit SM; Ruotolo BT An Improved Calibration Approach for Traveling Wave Ion Mobility Spectrometry: Robust, High-Precision Collision Cross Sections. Anal. Chem 2021, 93 3542–3550. [PubMed: 33555172]

(52). Habibi SC; Nagy G Assessing the use of host-guest chemistry in conjunction with cyclic ion mobility separations for the linkage-specific characterization of human milk oligosaccharides. Int. J. Mass Spectrom 2023, 483.

(53). Giles K; Ujma J; Wildgoose J; Pringle S; Richardson K; Langridge D; Green M A Cyclic Ion Mobility-Mass Spectrometry System. Anal. Chem 2019, 91 8564–8573. [PubMed: 31141659]

(54). de Bruin CR; Hennebelle M; Vincken JP; de Bruijn WJC Separation of flavonoid isomers by cyclic ion mobility mass spectrometry. Anal. Chim. Acta 2023, 1244.

(55). McKenna KR; Li L; Baker AG; Ujma J; Krishnamurthy R; Liotta CL; Fernandez FM Carbohydrate isomer resolution via multi-site derivatization cyclic ion mobility-mass spectrometry. Analyst 2019, 144 7220–7226. [PubMed: 31670330]

(56). Ollivier S; Tarquis L; Fanuel M; Li A; Durand J; Laville E; Potocki-Veronese G; Ropartz D; Rogniaux H Anomeric Retention of Carbohydrates in Multistage Cyclic Ion Mobility (IMSn): De Novo Structural Elucidation of Enzymatically Produced Mannosides. Anal. Chem 2021, 93 6254–6261. [PubMed: 33829764]

(57). Breen J; Hashemihedeshi M; Amiri R; Dorman FL; Jobst KJ Unwrapping Wrap-around in Gas (or Liquid) Chromatographic Cyclic Ion Mobility-Mass Spectrometry. Anal. Chem 2022, 94 11113–11117. [PubMed: 35913896]

(58). Stow SM; Causon TJ; Zheng XY; Kurulugama RT; Mairinger T; May JC; Rennie EE; Baker ES; Smith RD; McLean JA; et al. An Interlaboratory Evaluation of Drift Tube Ion Mobility-Mass Spectrometry Collision Cross Section Measurements. Anal. Chem 2017, 89 9048–9055. [PubMed: 28763190]

(59). Forsythe JG; Petrov AS; Walker CA; Allen SJ; Pellissier JS; Bush MF; Hud NV; Fernandez FM Collision cross section calibrants for negative ion mode traveling wave ion mobility-mass spectrometry. Analyst 2015, 14 6853–6861.

(60). Ruotolo BT; Benesch JLP; Sandercock AM; Hyung SJ; Robinson CV Ion mobility-mass spectrometry analysis of large protein complexes. Nat. Protoc 2008, 3 1139–1152. [PubMed: 18600219]

(61). Zhou ZW; Shen XT; Tu J; Zhu ZJ Large-Scale Prediction of Collision Cross-Section Values for Metabolites in Ion Mobility-Mass Spectrometry. Anal. Chem 2016, 88 11084–11091. [PubMed: 27768289]

(62). Hines KM; Ross DH; Davidson KL; Bush MF; Xu LB Large-Scale Structural Characterization of Drug and Drug-Like Compounds by High-Throughput Ion Mobility-Mass Spectrometry. Anal. Chem 2017, 89 9023–9030. [PubMed: 28764324]

(63). Picache JA; Rose BS; Balinski A; Leaptrot KL; Sherrod SD; May JC; McLean JA Collision cross section compendium to annotate and predict multi-omic compound identities. Chem. Sci 2019, 10 983–993. [PubMed: 30774892]

(64). Zheng XY; Aly NA; Zhou YX; Dupuis KT; Bilbao A; Paurus VL; Orton DJ; Wilson R; Payne SH; Smith RD; et al. A structural examination and collision cross section database for over 500 metabolites and xenobiotics using drift tube ion mobility spectrometry. Chem. Sci 2017, 8 7724–7736. [PubMed: 29568436]

(65). Yamabe S; Ishikawa T Theoretical study of mutarotation of glucose. J. Org. Chem 1999, 64 4519–4524.

(66). Pigman W; Isbell HS Mutarotation of sugars in solution. 1. History, basic kinetics, and composition of sugar solutions. Adv. Carbohydr. Chem. Biochem 1968, 23 11–57. [PubMed: 4882954]

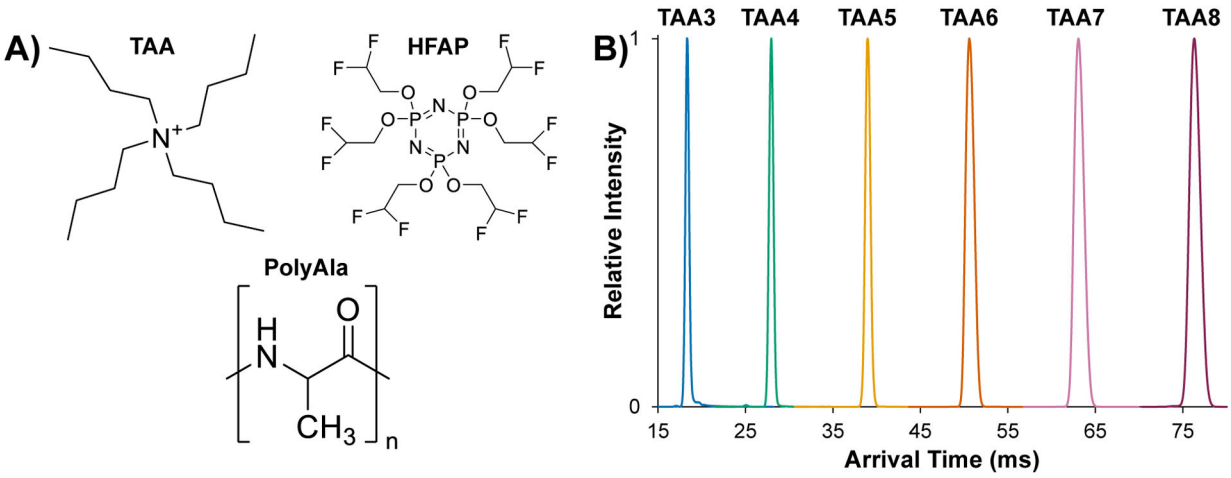

Figure 1.

Structure of calibrants: tetraalkylammonium salts [TAA; tetrabutylammonium shown], polyalanine [PolyAla] and hexakis(fluoroalkoxy)phosphazines [HFAP; hexakis(2,2-difluoroethoxy)phosphazine shown] (A). Arrival time distributions of TAA3–8 as their [M+] at 4 m at TW conditions of 450 m/s and 22 V (B).

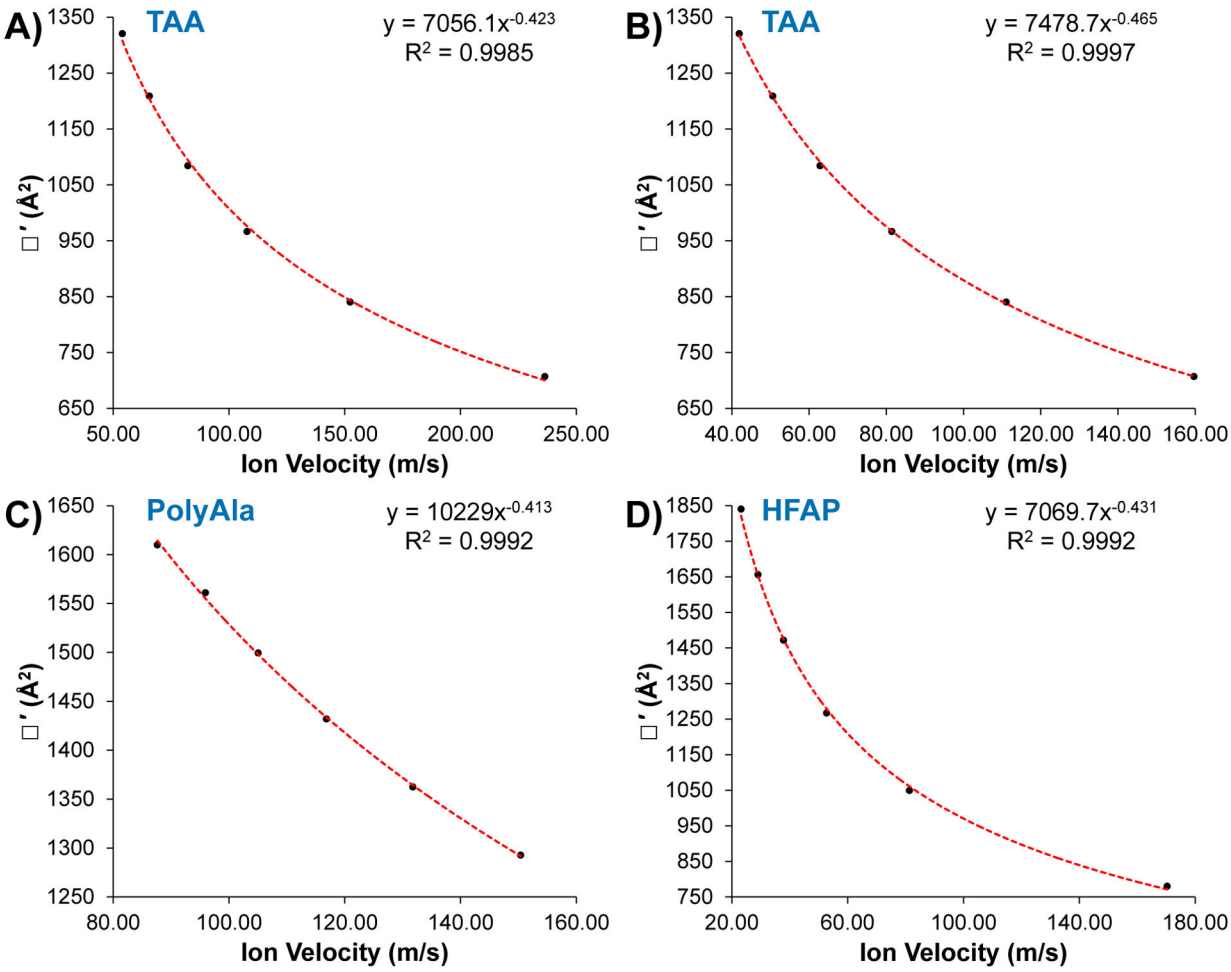

Figure 2.

The cIMS CCS calibration curves of TAAs at TW conditions of 450 m/s and 22 V (A) and 700 m/s and 25 V (B), PolyAla at TW conditions of 450 m/s and 35 V (C) and HFAP at TW conditions of 550 m/s and 24 V (D). We reiterate that these calibration curves were generated by averaging the ion velocities over several pathlengths and over three days. The reduced CCS values taken from these calibration curves were used to calculate average cIMS CCS values shown in Table 2 according to Equation 3.

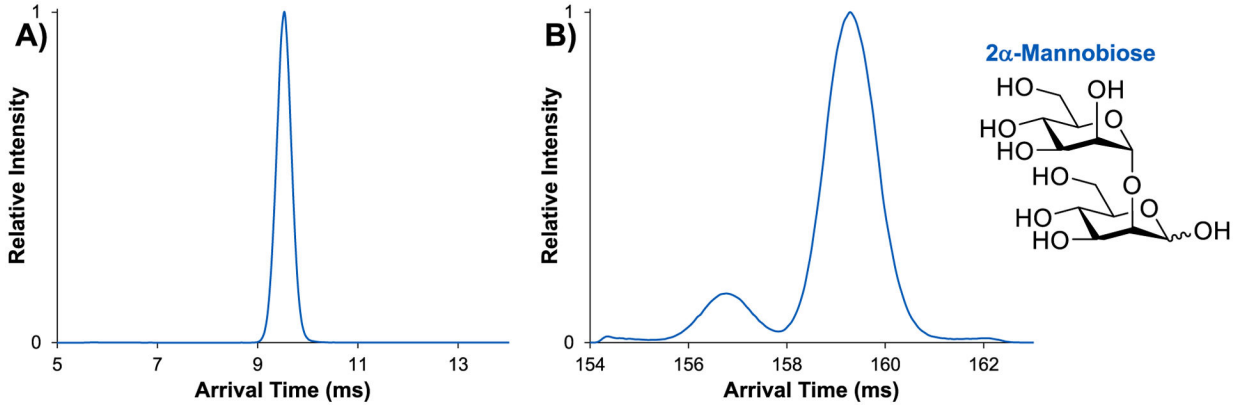

Figure 3.

The cIMS-MS separations of 2α-mannobiose as its $[M + Na]^+$ adduct at 1 m (A) and 20 m (B) at traveling wave conditions of 550 m/s and 24 V. We note the minor mobility features at ~ 154 and 162 ms are from the ion lapping/wrap-around effect.

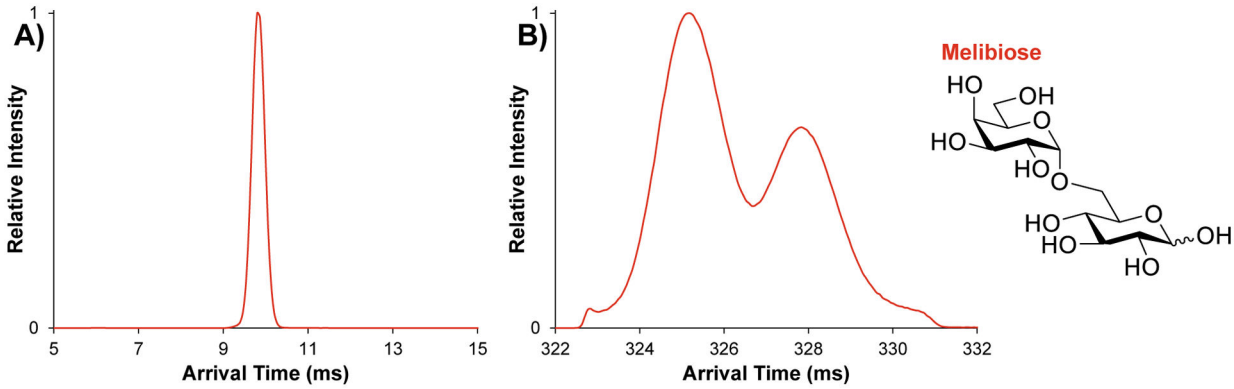

Figure 4.

cIMS-MS separations of melibiose as its $[M + Na]^+$ adduct at 1 m (A) and 40 m (B) at traveling wave conditions of 550 m/s and 24 V. We note the minor mobility features at ~ 323 and 331 ms are from the ion lapping/wrap-around effect.

Table 1.

TW conditions, *m/z* values, and calculated average ion velocities for calibrant species based on triplicate trials performed on three independent days. Please see Table S2 for pathlengths used to calculate ion velocities for each calibrant set.

TW Conditions	Calibrant	*m/z*	Average Ion Velocity (m/s)
450 m/s & 22 V	TAA3	186.2	236.4 ± 1.5
	TAA4	242.3	152.3 ± 0.7
	TAA5	298.3	107.8 ± 0.6
	TAA6	354.4	82.3 ± 0.2
	TAA7	410.5	65.6 ± 0.1
	TAA8	466.5	53.9 ± 0.1
700 m/s & 25 V	TAA3	186.2	159.7 ± 0.2
	TAA4	242.3	111.1 ± 0.3
	TAA5	298.3	81.4 ± 0.2
	TAA6	354.4	62.8 ± 0.1
	TAA7	410.5	50.6 ± 0.1
	TAA8	466.5	41.9 ± 0.1
450 m/s & 35 V	A10	729.4	150.4 ± 0.7
	A11	800.4	131.8 ± 0.7
	A12	871.5	116.8 ± 0.3
	A13	942.5	105.0 ± 0.3
	A14	1013.5	95.9 ± 0.3
	A15	1084.6	87.6 ± 0.3
550 m/s & 24 V	$HFAP_{322}$	322.0	170.3 ± 0.3
	$HFAP_{622}$	622.0	81.4 ± 0.2
	$HFAP_{922}$	922.0	52.7 ± 0.1
	$HFAP_{1222}$	1222.0	37.8 ± 0.1
	$HFAP_{1522}$	1522.0	29.1 ± 0.0
	$HFAP_{1822}$	1822.0	23.2 ± 0.0

Table 2.

Average cIMS CCS values obtained from our calibration curves (Figure 2), and comparison to previously published DTIMS CCS values for these calibrants. DTIMS CCS for TAAs and PolyAla were obtained from Reference 47, and HFAP was obtained from Reference 58.

TW Conditions	Calibrant	Average cIMS CCS (Å^2)	DTIMS CCS[47, 58] (Å^2)	cIMS vs DTIMS Error (%)
450 m/s & 22 V	TAA3	141.7 ± 0.4	143.3	−1.1
	TAA4	168.0 ± 0.3	167.7	0.2
	TAA5	192.6 ± 0.5	191.0	0.8
	TAA6	214.5 ± 0.2	212.8	0.8
	TAA7	234.8 ± 0.2	236.1	−0.6
	TAA8	254.1 ± 0.2	256.9	−1.1
700 m/s & 25 V	TAA3	143.3 ± 0.1	143.3	0.0
	TAA4	167.0 ± 0.2	167.7	−0.4
	TAA5	191.0 ± 0.2	191.0	0.0
	TAA6	214.0 ± 0.2	212.8	0.6
	TAA7	235.6 ± 0.2	236.1	−0.2
	TAA8	256.1 ± 0.3	256.9	−0.3
450 m/s & 35 V	A10	248.4 ± 0.5	248.9	−0.2
	A11	261.9 ± 0.6	261.9	0.0
	A12	274.9 ± 0.3	274.9	0.0
	A13	286.9 ± 0.3	287.5	−0.2
	A14	297.6 ± 0.4	299.0	−0.5
	A15	308.6 ± 0.4	308.1	0.2
550 m/s & 24 V	$HFAP_{322}$	152.1 ± 0.1	153.7	−1.0
	$HFAP_{622}$	205.1 ± 0.2	202.7	1.2
	$HFAP_{922}$	245.5 ± 0.2	243.1	1.0
	$HFAP_{1222}$	282.2 ± 0.3	281.3	0.3
	$HFAP_{1522}$	315.5 ± 0.1	315.8	−0.1
	$HFAP_{1822}$	347.1 ± 0.3	350.4	−0.9

Table 3.

Summary of traveling wave conditions and cIMS CCS values for 2α-mannobiose and melibiose with multiple calibrants. The average cIMS CCS reported here represents an average of three trials performed on three separate days.

Glycans $[M + Na]^+$	Calibrant & TW Conditions	Average cIMS CCS (Å^2)		DTIMS CCS (Å^2)	TWIMS CCS (Å^2)
2α-mannobiose	TAA (450 m/s & 22 V)	Peak 1	170.5 ± 0.5	173.7[63] 174.8[64]	N/A
		Peak 2	171.8 ± 0.5		
	TAA (700 m/s & 25 V)	Peak 1	170.3 ± 0.4		
		Peak 2	171.5 ± 0.4		
	HFAP (550 m/s & 24 V)	Peak 1	170.3 ± 0.4		
		Peak 2	171.5 ± 0.4		
Melibiose	TAA (450 m/s & 22 V)	Peak 1	174.3 ± 0.3	177.1[63] 181.1[64] 176.8[61]	174.8[62]
		Peak 2	175.0 ± 0.4		
	TAA (700 m/s & 25 V)	Peak 1	173.7 ± 0.3		
		Peak 2	174.4 ± 0.3		
	HFAP (550 m/s & 24 V)	Peak 1	173.6 ± 0.2		
		Peak 2	174.3 ± 0.2		